RSC Advances

ROYAL SOCIETY OF CHEMISTRY

www.rsc.org/advances

Site occupancy and photoluminescence properties of Eu^{3+}-activated $Ba_2ZnB_2O_6$ phosphor

Huan Yi[a], Fang Li[a], Li Wu[a,*], Liwei Wu[a], Hongrun Wang[b], Biao Wang[b], Yi Zhang[b,*], Yongfa Kong[a], and Jingjun Xu[a]

a The MOE key laboratory of weak-Light Nonlinear Photonics, School of Physics, Nankai University, Tianjin 300071. Email: lwu@nankai.edu.cn; Tel: +86-22-23506257, Fax: +86-22-23505409

b Institute of Photo-electronic Thin Film Devices and Key Laboratory of Optoelectronic Information Science and Technology, Ministry of Education, Nankai University, Tianjin 300071, China. Email: yizhang@nankai.edu.cn, Tel: +86-22-23508572-8018, Fax: +86-22-23508912

Abstract

A series of $Ba_2ZnB_2O_6:Eu^{3+}$ phosphors with a red-emitting band centered at 616 nm were prepared by traditional high temperature solid-state reaction method. The site-preferred occupancy of Eu^{3+} in $Ba_2ZnB_2O_6$ and luminescence properties of $Ba_2ZnB_2O_6:Eu^{3+}$ were studied combined by X-ray diffraction (XRD), photoluminescence excitation (PLE) spectra and emission (PL) spectra as well as temperature-dependent PL and decay curves. The Rietveld refinements indicate that the Eu^{3+} ions prefer to occupy Zn (1) (4a) and Zn (2) (4a) sites simultaneously. The PL intensity is improved with increasing Eu^{3+} content and the optimal dopant content is 0.05. The temperature-dependent PL spectra indicate that the emission intensity decreases with the temperature because of the enhancement of the non-radiative transition. The PL emission intensities of $Ba_2ZnB_2O_6:0.05Eu^{3+}$ phosphors with Li^+, Na^+ and K^+ as charge compensators are enhanced significantly, and the phosphor compensated by Li^+ ions emits the strongest emission. The Commission Internationale de I'Eclairage (CIE) color coordinates of $Ba_2ZnB_2O_6:0.05Eu^{3+}$ is very close to the CIE of standard red light.

1. Introduction

Borate system comprises more than 500 kinds of structures due to the different combination modes of the B-O groups. [1,2] Because of the relative low synthesizing temperature, stable physical and chemical properties, and excellent luminescence performance,[3,4] borates have been a hot research topic in the field of luminescent host materials recently.

Eu^{3+} is an important rare earth ion in synthesizing phosphors with good properties, for example $Y_2O_3:Eu^{3+}$ is used as red phosphor in wLEDs. Recently, many types of Eu^{3+}-doped compounds have been reported as interesting candidates for potential red-emitting phosphors. [5-11] Because of the proper ionic radii of Ba^{2+} and Zn^{2+}, a series of barium containing compounds and zinc containing compounds have been used as host materials to be doped by Eu^{3+}, such as $Ba_{1-x}B_8O_{13}:xEu^{3+}$,[12] $Ba_{5-2x}(VO_4)_3Cl:xEu^{3+},xK^+$,[13] $Zn_{1-x}AlO_4$: xEu^{3+} [14] and $Zn_{1-x-y}B_2O_4:xBi^{3+},yEu^{3+}$,[15] and so on. The radius of Ba^{2+} ion is larger than that of Eu^{3+} ion, and Zn^{2+} ion is smaller than that of Eu^{3+}. However, Eu^{3+} can occupy Ba^{2+} sites or Zn^{2+} sites in different hosts. For example, Eu^{3+} ions occupy Ba^{2+} site in $Ba_{1-x}B_8O_{13}$ doped by Eu^{3+},[10] but occupy Zn^{2+} site in $Zn_{1-x-y}B_2O_4$ codoped by $Bi^{3+}$and Eu^{3+}.[15]

As one of alkaline earth borates, $Ba_2ZnB_2O_6$ was firstly synthesized by Robert and Koliha in 1994.[16] This compound crystallizes in *Pca2₁* space group with a=15.068(2), b=8.720(2), c=10.128(3) Å, and V=1330.7 (9) $Å^3$. There are four different Ba^{2+} ions sites, two different Zn^{2+} ions sites and three different B^{3+} ions sites in this compound. Two different groups, vertex-sharing ZnO_4 tetrahedra and BO_3 triangles, constitute two-dimensional $[Zn_3B_3O_6]_\infty$ layers which are perpendicular to the [100] direction in the $Ba_2ZnB_2O_6$ structure. The layers are linked by the additional BO_3 groups, forming a 3D framework. The Ba^{2+} ions fill the space of the 3D

framework to balance the charge. All the BO_3 groups in the layers are parallel with each other throughout the structure. The structure of $Ba_2ZnB_2O_6$ indicates that this compound can offer a proper host structure environment for the doped Eu^{3+} ions. As mentioned above, the doped Eu^{3+} can occupy Ba^{2+} sites or Zn^{2+} sites in the Ba-based borates or Zn-based borates. However, $Ba_2ZnB_2O_6$ contains Ba^{2+} and Zn^{2+} ions. The site occupancy and the photoluminescence properties of Eu^{3+} ions in such Ba and Zn co-containing compounds are not studied before. In this study, Eu^{3+} activated $Ba_2ZnB_2O_6$ phosphors are prepared and the site occupancy of Eu^{3+} in $Ba_2ZnB_2O_6$ is studied as well as the photoluminescence properties of Eu^{3+} activated $Ba_2ZnB_2O_6$ phosphors. In order to eliminate the charge unbalance because of Eu^{3+} doped into $Ba_2ZnB_2O_6$, the effect of charge compensation is also studied in this paper.

2. Experimental

Polycrystalline samples of $Ba_2ZnB_2O_6:Eu^{3+}$ and $Ba_2ZnB_2O_6:Eu^{3+}$, M^+ (M=Li, Na and K) were prepared by a solid-state reaction at high temperature starting from analytical purity $BaCO_3$, ZnO, H_3BO_3 and Eu_2O_3, Li_2CO_3, Na_2CO_3, and K_2CO_3 (99.99%). The raw materials were weighed out, mixed and ground together in an agate mortar, and then sintered at 600 ^oC for 24 h in air to remove the H_2O and CO_2 in a muffle furnace. After cooled down to room temperature, the samples were ground again and further sintered at 800 ^oC for 72 h in air.

The X-ray diffraction (XRD) data for phase identification of the as-prepared powders were collected in the range of 10° to 80° on a PANalytical X'Pert Pro powder X-ray diffractometer with Cu Kα radiation (40 kV, 40 mA). The XRD for structure refinement were collected over a 2ϑ range from 10° to 140° at intervals of 0.017° with a counting time of 1 s per step. The photoluminescence (PL) and photoluminescence excitation (PLE) spectra of the samples were

measured by a spectrofluorometer (Edinburgh Instruments, FLS920) equipped with a Xe light source and double excitation monochromators. The powder samples were placed into circular sample cells with quartz plates and excited under 45° incidences. The emitted fluorescence was detected by a photomultiplier (R928P) that is perpendicular to the excitation beam. A cutoff filter was used to avoid the influence of the second-order emission of the source radiation. Diffuse reflectance spectra of the phosphors were measured by a UV-visible spectrophotometer (Hitachi U-4100). The lifetimes were recorded using a μF900 lamp (100 W) as a light source and a photomultiplier (R928P) was used as detector. The temperature-dependent luminescence properties were measured on a fluorescence spectrophotometer (F-4600, HITACHI, Japan) with a photomultiplier tube operating at 400 V, and a 150 W Xe lamp used as the excitation lamp.

3. Results and discussion

3.1 Site-preferred occupancy of the $Ba_2ZnB_2O_6$:xEu^{3+}

The phase purities of $Ba_2ZnB_2O_6$:xEu^{3+} (x=0-0.08) were confirmed by X-ray diffraction (XRD) at room temperature, as shown in Fig. 1. The XRD patterns are found to be in good agreement with that was reported by Smith *et al.* in 1994,[16] which indicates that the structure of host is not changed by doping Eu^{3+} ions regardless of Eu^{3+} contents.

As introduced above, $Ba_2ZnB_2O_6$ crystallizes in an orthorhombic system with space group $Pca2_1$, and offers two types of ions for Eu^{3+} to replace: four-coordinated Zn^{2+} ions and six- or seven-coordinated Ba^{2+} ions. Considering the ionic radius (r) of different coordination number (CN) reported by Shannon,[17] the ionic radius changes with the coordination number. The radius of Zn^{2+} is r=0.60 Å as CN=4, and the radius of Ba^{2+} is r=1.35 Å as CN=6 and r=1.38 Å as CN=7, respectively. However, the radius of the doped Eu^{3+} is r=0.89 Å as CN=4, r=0.947 Å as CN=6, and

r=1.01 Å as CN=7. Compared with the radii of Zn^{2+} and Ba^{2+}, the doped Eu^{3+} will prefer to occupy Zn^{2+} site. The radius of Ba^{2+} is much larger than that of Eu^{3+} (the difference between of these two ions is 0.403 Å as CN=6 and 0.37 Å as CN=7), which will result in the crystal structure distortion of $Ba_2ZnB_2O_6$ too much to be stable in crystallography if the Ba^{2+} site is occupied by Eu^{3+}. Therefore, it is expected that Eu^{3+} will not prefer to occupy Ba^{2+} sites in this compound.

Rietveld refinement was proposed by H. Rietveld in 1967. Refinement of the structure parameters from diffraction data can obtain the crystal structure properties, such as the lattice parameters, the atomic positions of the doped ions, and occupancies.[18,19] In order to prove the Eu^{3+} ions occupy Zn^{2+} sites in $Ba_2ZnB_2O_6:Eu^{3+}$, the refinement of the XRD patterns of $Ba_2ZnB_2O_6:Eu^{3+}$ by Rietveld method [20,21] within the Fullprof Program [22] were performed. It is found that the Ba^{2+} sites cannot be occupied because of the final agreement factors are very high and the occupancy of Eu^{3+} on this site is far away from the nominal doping content. As for Zn^{2+} sites, it is found that all the doped Eu^{3+} ions are preferred to occupy Zn(1) (4*a*) site and Zn(2) (4*a*) sites during the refinement. Table 1 summarizes the lattice parameters and agreement factors for $ZnBi_2B_2O_7:xEu^{3+}$ (x=0.01-0.08) refined by Rietveld method. Fig. 2(a) shows the selected Rietveld refinement plot of $Ba_2ZnB_2O_6:0.05Eu^{3+}$. Fig. 2(b) shows the structure of $Ba_2ZnB_2O_6$ and Fig. 2(c) shows two different Zn^{2+}/Eu^{3+} coordination environment. The final agreement is converged to R_p=5.97%, R_{wp}=7.95%, and R_{exp}=3.73%. The refinement results indicate that $Ba_2ZnB_2O_6:0.05Eu^{3+}$ crystallizes in Orthorhombic system with a space group $Pca2_1$ and the lattice parameters a=15.1104(4) Å, b=8.7218(2) Å, c=10.1341(3) Å, and cell volume=1336.010 (2) $Å^3$. The longer lattice parameters of $Ba_2ZnB_2O_6$ doped by Eu^{3+} is because of the fact that $r_{Eu^{3+}} > r_{Zn^{2+}}$. The atomic positions in the doped $Ba_2ZnB_2O_6:0.05Eu^{3+}$ unit cell are

shown in Table S1. The refined concentration of Eu^{3+} is 5.3%, which is in good agreement with the original doping concentration of 5%. The refinement results confirm that Eu^{3+} ions prefer to occupy Zn1(4a) site and Zn2(4a) site, which means Eu^{3+} is coordinated by four O^{2-} with a tetrahedral crystal field environment.

3.2 Diffuse reflectance spectra

Because the powder of $Ba_2ZnB_2O_6$:Eu^{3+} is opaque, diffuse reflectance spectra (DRS) of the parent $Ba_2ZnB_2O_6$ and doped $Ba_2ZnB_2O_6$:0.05Eu^{3+} phosphor were measured instead of absorption spectra. As shown in Fig. 3, the diffuse reflectance spectrum of undoped sample shows obvious decrease from 240 nm to 370 nm near UV-region, which is due to the boron to oxygen charge transition (CT) in $Ba_2ZnB_2O_6$. When introducing the Eu^{3+} ions, the $Ba_2ZnB_2O_6$:0.05Eu^{3+} sample reveals stronger absorption than the undoped sample in this range. The stronger absorption is possibly caused by the energy transfer from borate groups to Eu^{3+} ions and CT transition of O^{2-}-Eu^{3+} in $Ba_2ZnB_2O_6$:0.05Eu^{3+} phosphor. In careful observation, the absorption in the range of 390~470 nm has a slight decrease compared with the undoped sample (upper inset in Fig. 3), which is ascribed to the typical *4f-4f* transition absorption of Eu^{3+}. The characteristic absorption bands of Eu^{3+} are not observed besides of the weak band centered at 466 nm ($^7F_0$-$^5D_2$ transition).

The absorption spectra of undoped and $Ba_2ZnB_2O_6$:0.05Eu^{3+} samples are also calculated by the Kubelka-Munk function:[23]

$$F(R) = (1-R)^2 / 2R = K/S \quad (1)$$

where *R*, *K* and *S* represent the reflection, absorption, and scattering coefficient, respectively. The absorption spectra are displayed in the below inset of Fig. 3. The $Ba_2ZnB_2O_6$:0.05Eu^{3+}

sample shows strong absorption from 240 nm to 370 nm, which is consistent with the diffuse reflectance spectra.

3.3 PLE and PL spectra

The PLE and PL spectra of $Ba_2ZnB_2O_6$:0.05Eu^{3+} are shown in Fig. 4(a). As can be seen in this figure, the PLE spectrum (recorded at 616 nm emission, black line) contains a broad band and a series of narrow bands locating in the range of ~240-480 nm, which is associated with the absorption spectrum (Fig. 3). The broad band at 240-320 nm originates from the charge transfer (CT) transition of O^{2-}-Eu^{3+}.[24] Those narrow bands belong to the typical *4f-4f* transition absorption bands of Eu^{3+}, in which the two intense bands centered at 393 nm and 466 nm are attributed to $^7F_0$-$^5L_6$ and $^7F_0$-$^5D_2$ transition. This demonstrates that the phosphor can be excited efficiently by near-ultraviolet and blue light. The other excitation peaks centered at 319 nm, 362 nm, 376 nm, 383 nm, 398 nm, and 415 nm correspond to the transitions from $^7F_0$ to $^5H_6$, $^5D_4$, $^5G_3$, $^5L_7$, $^5L_6$, and $^5D_3$ levels, respectively.

The PL spectrum (excited at 393 nm, red line) in Fig. 4(a) shows a series of sharp bands from 579 nm to 621 nm corresponding to the $^5D_0$-^7F_J (J=0, 1, 2) transitions of Eu^{3+}. According to the magnetic dipole (MD) transition selection rule (ΔJ=0, ±1), the emission band belonging to $^5D_0$-$^7F_1$ transition (ΔJ=1) is attributed to the magnetic dipole transition and the emission band belonging to $^5D_0$-$^7F_2$ is attributed to the electric dipole (ED) transition on the basis of the selection rule of electric dipole transition (ΔJ≤6, when J or J'=0, ΔJ=2, 4, 6). [15] The $^5D_0$-$^7F_0$ transition is forbidden and sensitive to the crystal field.[25] The weak emission peak centered at 579 nm belongs to the $^5D_0$-$^7F_0$ transition that is induced by role of crystal field in odd. The $^5D_0$-$^7F_0$ transition exists only when Eu^{3+} occupies sites with local symmetries of C_n, C_{nv} or C_s. So

we can deduce that Eu^{3+} occupies one site of C_n, C_{nv} or C_s symmetries.[26] The emission bands of Eu^{3+} in Fig. 4(a) are broadened and split into several lines, indicating that the ^7F_J levels appear Stark levels because of crystal field effect.[27, 28] The $^5D_0$-$^7F_1$ transition splits into two emission peaks centered at 590 nm and 594 nm, the $^5D_0$-$^7F_2$ transition splits into three emission peaks centered at 610 nm, 616 nm and 621 nm, and the $^5D_0$-$^7F_3$ transition splits into three emission peaks centered at 649 nm, 656 nm and 666 nm, respectively. Fig. 4(b) illustrates the partial energy diagram of Eu^{3+} ions in $Ba_2ZnB_2O_6$ host. For the excited state of Eu^{3+}, a fast non-radiation (NR) transition happened to the $^5D_0$ level, resulting the $^5D_{3,2,1}$-^7F_J transitions are restrained, so the emission of Eu^{3+} ions is thought to come from the $^5D_0$-^7F_J transitions.[29]

3.4 Concentration quenching

As seen in Fig. 5(a), the quenching concentration of $Ba_2ZnB_2O_6$:xEu^{3+} phosphors is 5 mol%. The emission intensity increases with increasing Eu^{3+} dopant content when x<0.05, while it decreases after that doping concentration. Based on the Dexter and Schulman theory,[30] concentration quenching is due to energy transfer from one activator to another until an energy sink is reached in the lattice. The concentration quenching in solid systems is because of the role of electric multipole or magnetic dipole interaction. On the basis of energy transfer formula:

$$I / x = k\left[1 + \beta\left(x\right)^{\theta/3}\right]^{-1} \quad (2)$$

where x is the mole fraction of activator ions; k and β are constants; I is the luminous intensity, and ϑ=6, 8, 10 corresponding to dipole-dipole, dipole-quadrupole, and quadrupole-quadrupole interactions, respectively. As illustrated in the inset of Fig. 5(b), the relationship of lg(I/x) versus lg(x) is linear and the slope of the line is about -2. So the value of ϑ is approximately equal to 6, which clearly indicates that the concentration quenching mechanism of Eu^{3+} in

$Ba_2ZnB_2O_6$:0.05Eu^{3+} is the dipole-dipole interaction.

Blasse[31] suggested that the critical distance (R_c) of energy transfer can be expressed by Eq. (3):

$$R_c \approx 2\left(3V / 4\pi x_c Z\right)^{1/3} \quad (3)$$

where x_c is the critical concentration of dopants, V is the volume of the unit cell, Z is the number of formula units per unit cell. As for $Ba_2ZnB_2O_6$ host, V=1336.010(2) Å^3, Z=8, and x_c=0.05, the calculated value of R_c is about 18.55 Å.

3.5. Temperature-dependent PL properties

Temperature-dependent PL spectra of $Ba_2ZnB_2O_6$:0.05Eu^{3+} are measured and displayed in Fig. 6(a). Because of the resolution of the fluorescence spectrophotometer used for temperature-dependent PL measurement, the splits of the emission peak $^5D_0$-$^7F_1$ and the $^5D_0$-$^7F_2$ cannot be distinguished clearly. With the temperature increasing, the emission intensities decrease fast, and the intensity at 150 ^oC only remains 30% of that at room temperature. The fast decrease of emission intensity with the increasing of temperature is possibly because of the non-radiative process. The non-radiative transition probability is strongly dependent on temperature. With the temperature increase, the non-radiative transition probability enhances greatly, which will result in the decrease of the emission intensity. It can also be found that the main emission peak wavelength shifts from 616 nm to 623 nm. To better understand the temperature dependence of photoluminescence and to determine the activation energy for thermal quenching, the Arrhenius equation is fitted to the thermal quenching data:[32]

$$I_T = I_0 / \left[1 + \exp(-E_a / kT)\right] \quad (4)$$

where I_0 and I_T are the luminescence intensities of $Ba_2ZnB_2O_6$:0.05Eu^{3+} at room temperature and the testing temperature, respectively. E_a is activation energy and k is the Boltzmann constant (8.617×10^{-5} eV K^{-1}). Fig. 6(b) plots $\ln(I_0/I_T-1)$ vs. $1/kT$ and the slope of the line is calculated to be -0.27. Therefore, E_a is obtained to be 0.27 eV.

3.6 Charge compensation

In $Ba_2ZnB_2O_6$:Eu^{3+}, the charge is not balanced because of the trivalent Eu^{3+} ions occupy the sites of the bivalent Zn^{2+} ions, which will introduce Zn vacancies or extra O^{2-} ions at nearby interstitial position. Each of these defects leads to the distortion of local environment symmetries of optical centers.[33] Therefore, alkali metal ions Li^+, Na^+ and K^+ are co-doped with Eu^{3+} in the matrix to balance the charge and reduce the variety of the activator symmetry sites. The PL spectra of $Ba_2ZnB_2O_6$:0.05Eu^{3+} and $Ba_2ZnB_2O_6$: 0.05Eu^{3+}, 0.05M (M= Li^+, Na^+ and K^+) under 393 nm excitation are shown in Fig. 7. No significant difference is observed between the emission peaks of $Ba_2ZnB_2O_6$:0.05Eu^{3+} and $Ba_2ZnB_2O_6$:0.05M, 0.05Eu^{3+} (M= Li^+, Na^+ and K^+) except the enhanced emission intensity. As shown in Fig. 7, the emission intensity compensated by Li^+ is strongest. The intensities of the emission peak centered at 616 nm for the phosphors doped by Li^+ and Na^+ as charge compensators are enhanced 1.61 and 1.41 times compared with the corresponding peak intensity for the phosphor without charge compensators, respectively. However, the emission intensity of the peak centered at 616 nm is almost unchangeable when the K^+ ions are added as charge compensation, which is considered to be caused by the huge difference between the K^+ and Zn^{2+} ionic radii. In $Ba_2ZnB_2O_6$:Eu^{3+}, Eu^{3+} ions have been proved to occupy the two four-coordinated Zn^{2+} sites. The ionic radii of Li^+, Na^+ and K^+ (CN=4) reported by Shannon [17] are 0.59 Å, 0.99 Å and 1.37 Å, respectively. Obviously, the ionic radius of Li^+ is very

close to the radius of Zn^{2+} (r=0.60 Å, CN=4), while K^+ is too large, which will be difficult to occupy Zn^{2+} sites. Therefore $Ba_2ZnB_2O_6$:0.05Eu^{3+} singly doped Li^+ as compensator shows the strongest emission intensity.

3.7 Decay properties and CIE coordinate

The decay curves of $Ba_2ZnB_2O_6$:0.05Eu^{3+} and $Ba_2ZnB_2O_6$:0.05Li^+, 0.05Eu^{3+} were measured and shown in Fig. 8 (a) and (b). The corresponding luminescence decay times of Eu^{3+} emission at 616 nm can be best expressed by the double exponential equation:[25]

$$I = I_0 + A_1 \exp(-t/\tau_1) + A_2 \exp(-t/\tau_2) \quad (5)$$

where I_0 and I represent the luminescence intensities when time is *0* and *t*, τ_1 and τ_2 are the fast and slow components of luminescent lifetime respectively, and A_1 and A_2 are the fitting parameters respectively. When there is no interaction between rare earth ions, the decay curve is usually a single exponential function. But both the decay curves of $Ba_2ZnB_2O_6$:0.05Eu^{3+} and $Ba_2ZnB_2O_6$: 0.05Eu^{3+}, 0.05Li^+ exhibit obvious deviations from the single exponential decay. As displayed in Fig. 8(a) and (b), the decay curves of $Ba_2ZnB_2O_6$:0.05Eu^{3+} and $Ba_2ZnB_2O_6$: 0.05Eu^{3+}, 0.05Li^+ are fitted well by the double exponential equation, which is one of the evidences that Eu^{3+} ions occupy the sites of both Zn(1) and Zn(2) and charge compensator does not change the site occupancy of Eu^{3+} in $Ba_2ZnB_2O_6$. The related fitting parameters are listed in Table. 2.

The effective decay lifetime is calculated by the following equation:

$$\tau = (A_1\tau_1^2 + A_2\tau_2^2)/(A_1\tau_1 + A_2\tau_2) \quad (6)$$

Based on Eq. (6), the average lifetimes of $Ba_2ZnB_2O_6$:0.05Eu^{3+} and $Ba_2ZnB_2O_6$:0.05Li^+ are 0.98 ms and 1.45 ms, respectively. The results indicate the decay times of $Ba_2ZnB_2O_6$:0.05Eu^{3+} and $Ba_2ZnB_2O_6$:0.05Li^+, 0.05Eu^{3+} are in the order of milliseconds.

The CIE coordinates of $Ba_2ZnB_2O_6$:0.05Eu^{3+} phosphors are calculated to be x = 0.655, y = 0.345, as shown in Fig. 9. The CIE coordinate of $Ba_2ZnB_2O_6$:0.05Eu^{3+} is very close to the CIE coordinate of standard red light (x = 0.67, y = 0.33), and is considered to be better than that of the commercial Y_2O_2S:Eu^{3+} (x = 0.622, y = 0.351). [34]

Table 3 summarizes the photoluminescence properties of some Ba-based and Zn-based hosts doped by Eu^{3+} as well as the data reported in this study. For those phosphors listed in Table 3, there is no big difference for their photoluminescence properties. The reported critical distance is around 15 nm for all the phosphors and the decay time is the magnitude of millisecond. The quenching mechanism are all dipole-dipole interaction for the phosphors listed in Table 3, which indicate that the different site occupancy for Eu^{3+} will not bring a big effect on the quenching mechanism of phosphors. However, emission color is different for these two different group phosphors. Compared with the red color emitted by Zn-based phosphor, the Ba-based phosphors emit the light from orange to red color ($^5D_0$-$^7F_1$ and $^5D_0$-$^7F_2$ transitions), which indicate that crystal environment will bring effect on the emission wavelength. When the large Eu^{3+} ion occupy Zn site, the volume of the crystal structure will be expanded and the polyhedron will be distorted, which will result in the increase the crystal field strength. As a consequence, a red shift will be observed in Zn-based phosphors.

4. Conclusion

In summary, the $Ba_2ZnB_2O_6$:Eu^{3+} phosphors were synthesized and investigated. The site-preferred occupancy of Eu^{3+} in $Ba_2ZnB_2O_6$ is studied by the Rietveld refinement. The doped Eu^{3+} ions prefer to occupy two Zn^{2+} sites. These phosphors can be excited efficiently by near-ultraviolet and blue light. The concentration quenching of the $Ba_2ZnB_2O_6$:xEu^{3+} phosphors

in the PL emission spectra optimized at 616 nm is x = 0.05. The PL emission intensities of $Ba_2ZnB_2O_6$:0.05Eu^{3+} phosphors compensated by Li^+, Na^+ and K^+ as charge compensators are enhanced, and the phosphors compensated by Li^+ ions show the strongest emission. The critical distance (R_c) and the lifetime value are determined to be 18.55 Å and 0.98 ms, respectively. The CIE coordinate is calculated to be x = 0.655, y = 0.345.

5. Acknowledgements

This work was financially supported by National Natural Science Foundation of China (51372121, 61274053, U146020005), Natural Science Foundation of Tianjin (14JCYBJC17800), the Program for New Century Excellent Talents in University of China (NCET-11-0258), and the Program for Changjiang Scholars and Innovative Research Team in University (IRT0149). We thank Mrs. Xu of N01 group, Institute of Physics, Chinese Academy of Science for her great help in collecting the powder X-ray diffraction data and Prof. Dr. Z. Xia for the great help of in the temperature-dependent PL spectra measurement.

Electronic Supplementary Information (ESI) available: Rietveld refinement results for $Ba_2ZnB_2O_6$:0.05Eu^{3+} phosphor. See DOI: 10.1039/b000000x/

References

[1] M. Touboul, N. Penin, G. Nowogrocki, Solid State Sci., 2003, **5**, 1327.

[2] FindIt, Version 1.3.3, ICSD database, 2004~02, FIZ Karlsruhe, Germany.

[3] L. Li, H. Liang, Z. Tian, H. Lin, Q. Su, G. Zhang, J. Phys. Chem. C, 2008, **112**, 13763.

[4] A. Shyichuk, S. Lis, J. Rare Earth., 2011, **29**, 1161.

[5] L. K. Bharat, B. V. Rao, J. S. Yu, Chem. Eng. J., 2014, **255**, 205.

[6] L. K. Bharat, J. S. Yu, J. Nanosci. Nanotechnol., 2013, **13**, 8239.

[7] Y. Huang, Y. Nakai, T. Tsuboi, H.J. Seo, Opt. Express, 2011, **19**, 6303.

[8] F. Lei, B. Yan, J. Solid State Chem., 2008, **181**, 855.

[9] S.-F. Wang, K. Koteswara Rao, Y.-R. Wang, Y.-F. Hsu, S.-H. Chen, Y.-C. Lu, J. Am. Ceram. Soc., 2009, **92**, 1732.

[10] L. Wu, Y. Zhang, M. Gui, P. Lu, L. Zhao, S. Tian, Y. Kong, J. Xu, J. Mater. Chem., 2012, **22**, 6463.

[11] Y. Zhang, L. Wu, M. Ji, B. Wang, Y. Kong, J. Xu, Opt. Mater. Express, 2012, **2**, 92.

[12] L. He, Y. Wang, W. Sun, J. Rare Earth., 2009, **27**, 385.

[13] Z. Xia, Y. Liang, W. Huang, M. Zhang, D. Yu, J. Wu, J. Zhao, M. Tong, Q. Wang, J. Mater. Sci.-Mater. Electron., 2013, **24**, 5111.

[14] V. Singh, V. Natarajan, J.-J. Zhu, Opt. Mater., 2007, **29**, 1447.

[15] W.-R. Liu, C.C. Lin, Y.-C. Chiu, Y.-T. Yeh, S.-M. Jang, R.-S. Liu, Opt. Express, 2010, **18**, 2946.

[16] R.W. Smith, L.J. Koliha, Mater. Res. Bull., 1994, **29**, 1203.

[17] R. Shannon, Acta Cryst. A, 1976, **32**, 751.

[18] L. Wu, M. Y. Ji, H. R. Wang, Y. F. Kong, Y. Zhang, Opt. Mater. Express, 2014, **4**, 1535.

[19] L. Wu, B. Wang, Y. Zhang, L. Li, H. R. Wang, H. Yi, Y. F. Kong, J. J. Xu, Dalton Trans., 2014, **43**, 13845.

[20] H. Rietveld, Acta Cryst., 1967, **22**, 151.

[21] H. Rietveld, J. Appl. Cryst., 1969, **2**, 65.

[22] J. Rodriguez-Carvajal, FULLPROF2000, (LLB, France, 2001).

[23] Y. Nobuhiko, J. Phys. Soc. Jpn., 1973, **35**, 1089.

[24] C.A. Kodaira, H.F. Brito, M.C.F. Felinto, J. Solid State Chem., 2003**, 171**, 401.

[25] G. Blasse, B. Grabmaier, Luminescent materials, Springer, 1994.

[26] X. Bai, G. Zhang, P. Fu, J. Solid State Chem., 2007, **180**, 1792.

[27] Y.-C. Li, Y.-H. Chang, Y.-F. Lin, Y.-S. Chang, Y.-J. Lin, J. Alloys Compd., 2007, **439**, 367.

[28] B. Liu, C. Shi, Z. Qi, Appl. Phys. Lett., 2005, **86**, 191111.

[29] G.V.L. Reddy, L.R. Moorthy, T. Chengaiah, B.C. Jamalaiah, Ceram. Int., 2014, **40**, 3399.

[30] D. Dexter, J. Schulman, J. Chem. Phys, 1954, **22**, 1063.

[31] G. Blasse, Philips Res. Rep, 1969, **24**, 131.

[32] R.-J. Xie, N. Hirosaki, N. Kimura, K. Sakuma, M. Mitomo, Appl. Phys. Lett., 2007, **90**, 191101.

[33] M. Puchalska, E. Zych, M. Sobczyk, A. Watras, P. Deren, Mater. Chem. Phys., 2014, **147**, 304.

[34] C. Guo, L. Luan, C. Chen, D. Huang, Q. Su, Mater.Lett., 2008, **62**, 600.

[35] J. Liu, X. D. Wang, Z. C. Wu, S. P. Kuang, Spectrochim. Acta Part A, 2011, **79**, 1520

[36] B. Han, P. Li, J. Zhang, H. Shi, J. Lumin. 2014, **155**, 15

Table 1. Lattice parameters and agreement factors for $ZnBi_2B_2O_7:xEu^{3+}$ (x=0.01-0.08) refined by Rietveld method.

Lattice parameter	X=0.01	X=0.02	X=0.03	X=0.04	X=0.05	X=0.06	X=0.07	X=0.08
a(Å)	15.0762(2)	15.0842(2)	15.0941(1)	15.1000(3)	15.1095(4)	15.1172(1)	15.1260(3)	15.1337(4)
b(Å)	8.7203(2)	8.7207(1)	8.7211(1)	8.7214(2)	8.7213(1)	8.7223(2)	8.7225(1)	8.7231(2)
c(Å)	10.1290(3)	10.1305(1)	10.1317(1)	10.1324(2)	10.1333(3)	10.1354(2)	10.1360(2)	10.1377(3)
V($Å^3$)	1331.61(3)	1332.67(2)	1333.69(1)	1334.35(3)	1335.57(4)	1336.42(2)	1337.31(3)	1338.30(4)
R_p(%)	5.43	5.68	5.88	5.84	5.97	6.12	6.22	6.21
R_{wp}(%)	7.57	7.67	7.80	7.76	7.95	8.22	8.37	8.40
R_{exp}(%)	3.70	3.70	3.73	3.73	3.73	3.73	3.74	3.74

Table 2. Constants (A) and Decay times (τ) of $Ba_2ZnB_2O_6:0.05Eu^{3+}$ and $Ba_2ZnB_2O_6:0.05Li^+$, $0.05Eu^{3+}$.

	A_1	A_2	τ_1(ms)	τ_2 (ms)	τ (ms)
$Ba_2ZnB_2O_6:0.05Eu^{3+}$	0.963	2.148	0.619	1.077	0.98
$Ba_2ZnB_2O_6:0.05Li^+,0.05Eu^{3+}$	1.506	2.130	1.565	1.360	1.45

Table 3. Luminescence properties including the position of emission peak, optimal concentration, critical distance and quenching mechanism for Eu^{3+} in some Ba-based and Zn-based hosts as well as that in $Ba_2ZnB_2O_6$.

host	*Strongest excited peak (nm)*	*Main transition*	*Optimal concentration*	*Critical distance (Å)*	*Quenching mechanism*	*Life time (ms)*	*ref*
$Ba_{5-2x}(VO_4)_3Cl$	466	$^5D_0$-$^7F_2$ (614nm)	0.22	--	Dipole-dipole	0.56	13
BaB_2O_4	394	$^5D_0$-$^7F_2$ (615nm)	0.06	14.56	Dipole-dipole	--	35
$KBaBP_2O_8$	394	$^5D_0$-$^7F_1$ (594nm)	0.1	15.2	Dipole-dipole	2.54	36
ZnB_2O_4	393	$^5D_0$-$^7F_2$ (621nm)	0.1	--	--	--	15
$Ba_2ZnB_2O_6$	393	$^5D_0$-$^7F_2$ (616nm)	0.05	18.55	Dipole-dipole	1.45	This work

Figure Captions

Fig. 1. XRD patterns of $Ba_2ZnB_2O_6$:xEu^{3+} (x=0.01-0.08).

Fig. 2. (a) Rietveld refinement plot on the XRD pattern of $Ba_2ZnB_2O_6$:0.05Eu^{3+}, small black circles and the red continuous lines represent the experimental and the calculated values respectively; vertical bars (|) indicate the position of Bragg peaks. The blue bottom trace depicts the corresponding residuals between the experimental and the calculated intensity values. (b) Crystal structure projection of $Ba_2ZnB_2O_6$ along c axis. (c) The coordination environments of two different Zn^{2+}/Eu^{3+} ions.

Fig. 3. Diffuse reflectance spectra of the parent and doped $Ba_2ZnB_2O_6$:0.05Eu^{3+} phosphors. Inset in the upper is the enlarged drawing on the peak centered at 465 nm. Inset in the below shows the absorption spectra (K/S) of $Ba_2ZnB_2O_6$ and $Ba_2ZnB_2O_6$:0.05Eu^{3+} derived with the Kubelka-Munk function.

Fig. 4. (a) PLE/PL spectra of the $Ba_2ZnB_2O_6$:0.05Eu^{3+} sample. (b) The energy level diagram for Eu^{3+} in $Ba_2ZnB_2O_6$.

Fig. 5. (a) PL spectrum of the $Ba_2ZnB_2O_6$:xEu^{3+} sample. (b) The emission intensity as a function of Eu^{3+} concentration in $Ba_2ZnB_2O_6$:xEu^{3+}. The inset is the dependence of lg (*I*/*x*) on lg (*x*).

Fig. 6. (a) Temperature-dependent PL spectra of $Ba_2ZnB_2O_6$:0.05Eu^{3+} phosphor (λ_{ex}=393 nm). (b) The $\ln(I_0/I_T-1)$ vs. $1/kT$ activation energy graph for thermal quenching of $Ba_2ZnB_2O_6$:0.05Eu^{3+}.

Fig. 7. PL spectra of $Ba_2ZnB_2O_6$:0.05Eu^{3+} and $Ba_2ZnB_2O_6$: 0.05M, 0.05Eu^{3+} (M= Li^+, Na^+ and K^+). (λ_{ex}=393 nm)

Fig. 8. (a) Decay curve of Eu^{3+} fluorescence in $Ba_2ZnB_2O_6$:0.05Eu^{3+}; (b) Decay curve of Eu^{3+} fluorescence $Ba_2ZnB_2O_6$:0.05Li^+, 0.05Eu^{3+}. (excited at 393 nm, monitored at 616 nm).

Fig. 9. CIE chromaticity diagram of $Ba_2ZnB_2O_6$:0.05Eu^{3+} phosphor under 393 nm excitation.

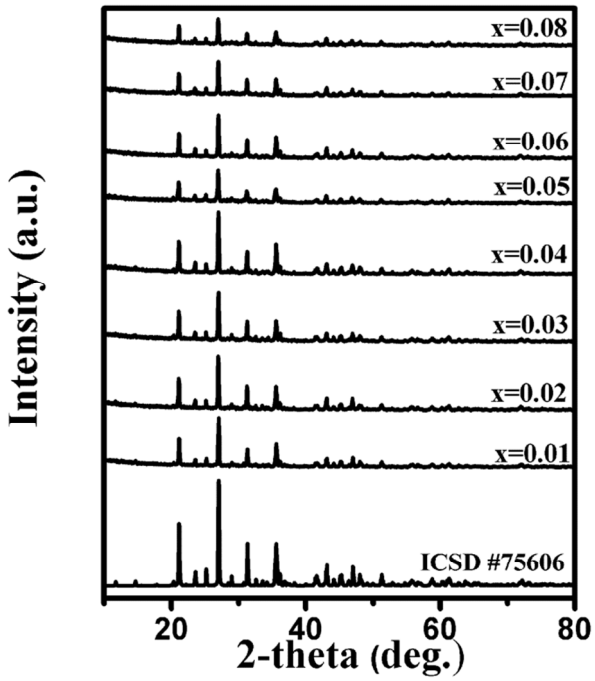

Fig. 1. XRD patterns of $Ba_2ZnB_2O_6:xEu^{3+}$ (x=0.01-0.08).

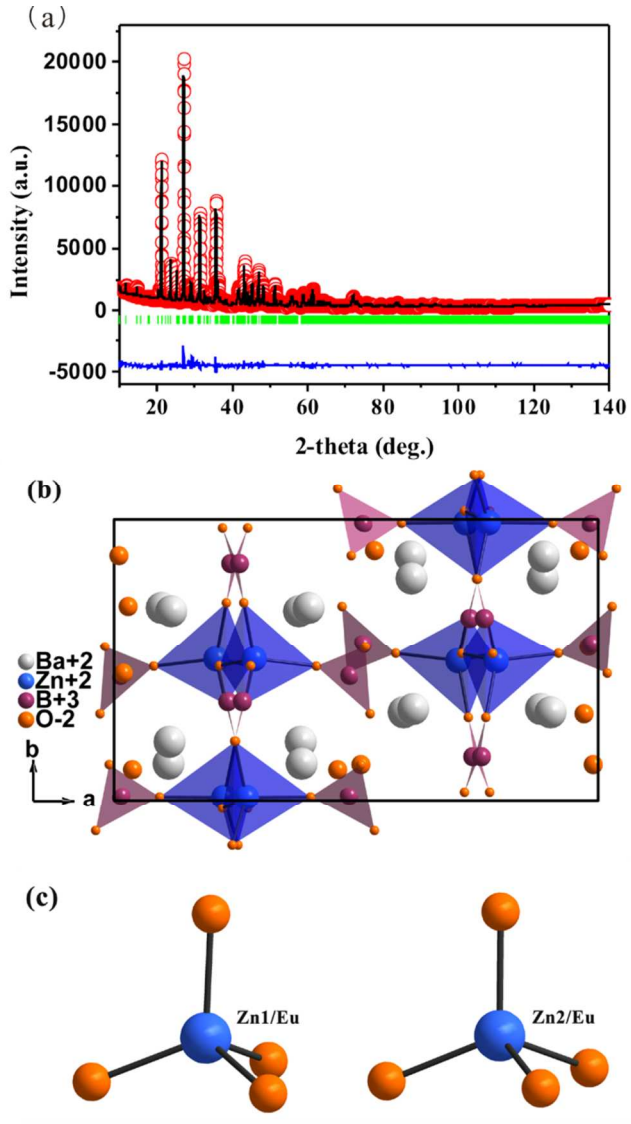

Fig. 2. (a) Rietveld refinement plot on the XRD pattern of $Ba_2ZnB_2O_6$:0.05Eu^{3+}, small black circles and the red continuous lines represent the experimental and the calculated values respectively; vertical bars (|) indicate the position of Bragg peaks. The blue bottom trace depicts the corresponding residuals between the experimental and the calculated intensity values. (b) Crystal structure projection of $Ba_2ZnB_2O_6$ along c axis. (c) The coordination environments of two different Zn^{2+}/Eu^{3+} ions.

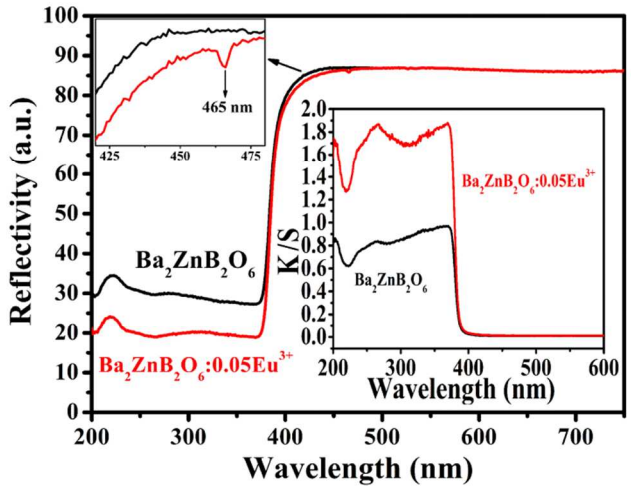

Fig. 3. Diffuse reflectance spectra of the parent and doped $Ba_2ZnB_2O_6$:0.05Eu^{3+} phosphors. Inset in the upper is the enlarged drawing on the peak centered at 465 nm. Inset in the below shows the absorption spectra (K/S) of $Ba_2ZnB_2O_6$ and $Ba_2ZnB_2O_6$:0.05Eu^{3+} derived with the Kubelka-Munk function.

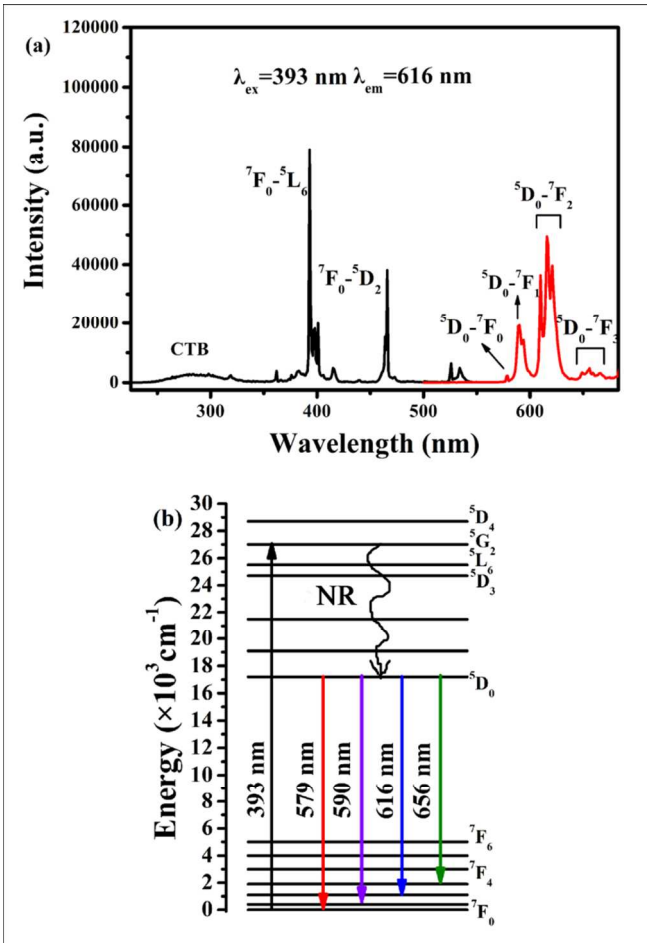

Fig. 4. (a) PLE/PL spectra of the $Ba_2ZnB_2O_6$:0.05Eu^{3+} sample. (b) The energy level diagram for Eu^{3+} in $Ba_2ZnB_2O_6$.

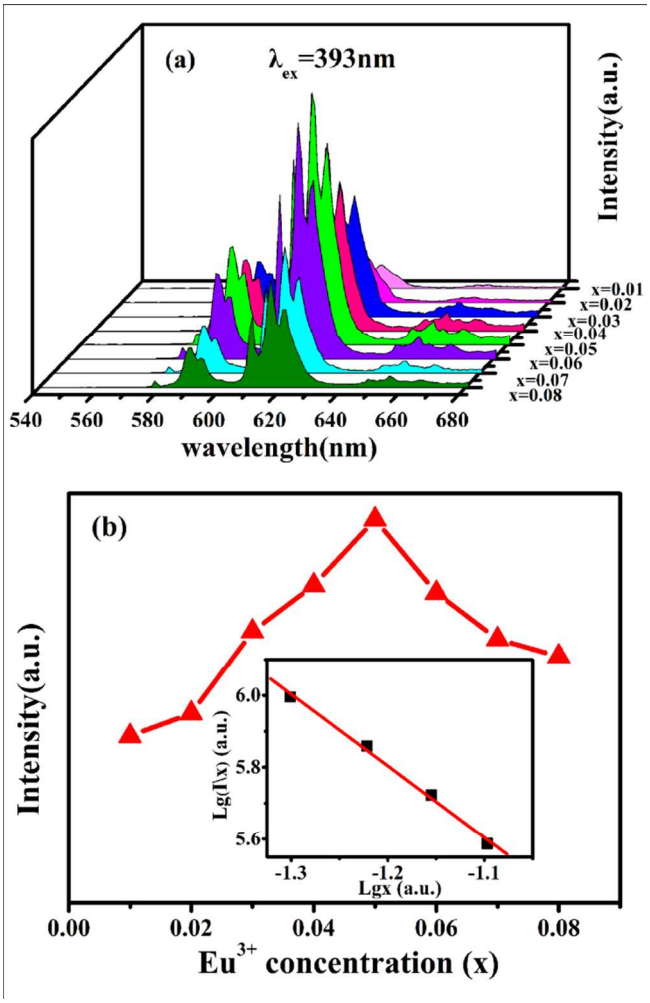

Fig. 5. (a) PL spectrum of the $Ba_2ZnB_2O_6$:xEu^{3+} sample. (b) The emission intensity as a function of Eu^{3+} concentration in $Ba_2ZnB_2O_6$:xEu^{3+}. The inset is the dependence of lg (*I*/*x*) on lg (*x*).

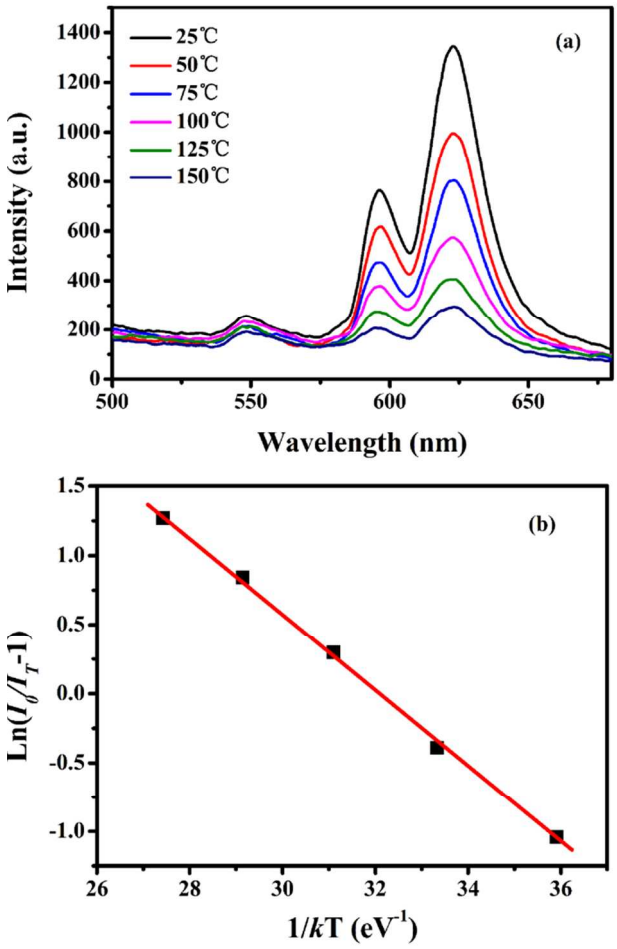

Fig. 6. (a) Temperature-dependent PL spectra of $Ba_2ZnB_2O_6$:0.05Eu^{3+} phosphor (λ_{ex}=393 nm). (b) The ln(I_0/I_T-1) vs. 1/kT activation energy graph for thermal quenching of $Ba_2ZnB_2O_6$:0.05Eu^{3+}.

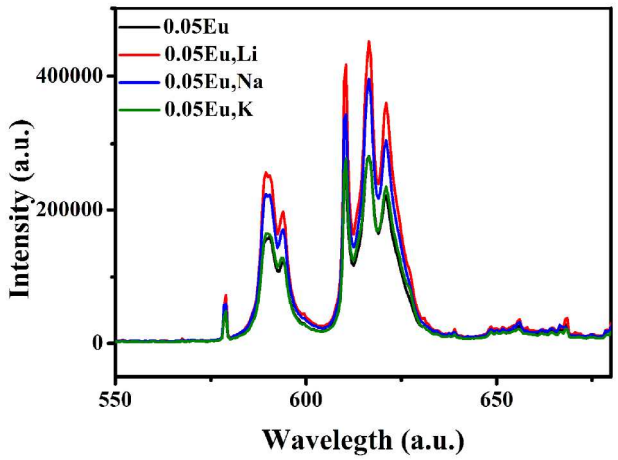

Fig. 7. PL spectra of $Ba_2ZnB_2O_6$:0.05Eu^{3+} and $Ba_2ZnB_2O_6$: 0.05M, 0.05Eu^{3+} (M= Li^+, Na^+ and K^+). (λ_{ex} =393 nm)

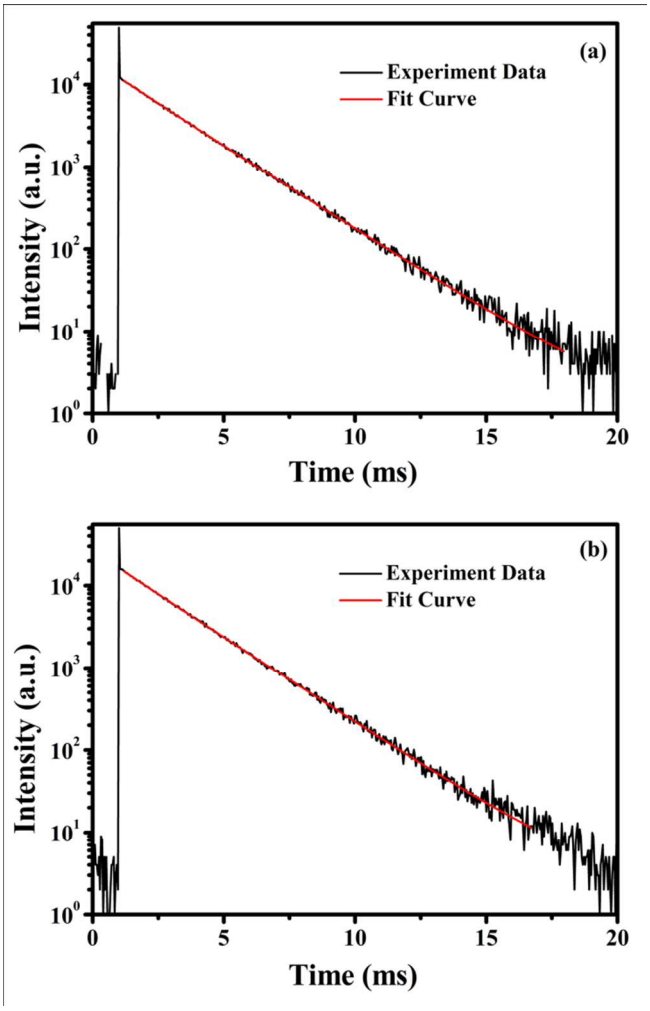

Fig. 8. (a) Decay curve of Eu^{3+} fluorescence in $Ba_2ZnB_2O_6$:0.05Eu^{3+}; (b) Decay curve of Eu^{3+} fluorescence $Ba_2ZnB_2O_6$:0.05Li^{+}, 0.05Eu^{3+}. (excited at 393 nm, monitored at 616 nm).

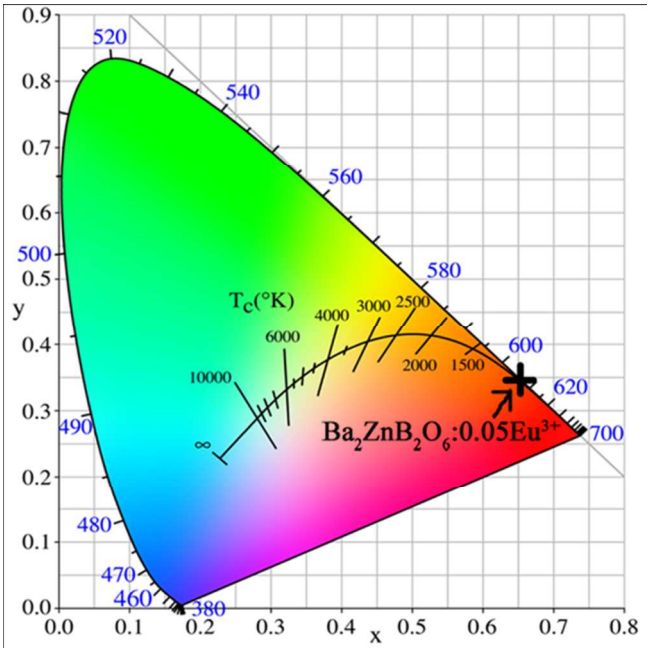

Fig. 9. CIE chromaticity diagram of $Ba_2ZnB_2O_6$:0.05Eu^{3+} phosphor under 393 nm excitation.